Cerebral Cortex, April 2020;30: 2281–2294

doi: 10.1093/cercor/bhz239
Advance Access Publication Date: 10 December 2019
Original Article

ORIGINAL ARTICLE

Reduced Microstructural Lateralization in Males with Chronic Schizophrenia: A Diffusional Kurtosis Imaging Study

Faye McKenna[1,2], James Babb[1], Laura Miles[1], Donald Goff[3] and Mariana Lazar[1,2]

[1]Department of Radiology, Center for Biomedical Imaging, New York, NY 10016, USA, [2]Sackler Institute of Graduate Biomedical Sciences New York University School of Medicine, New York, NY 10016, USA, and [3]Department of Psychiatry, New York University School of Medicine, New York, NY 10016, USA

Address correspondence to Faye McKenna, MS, Department of Radiology, New York University School of Medicine, Center for Biomedical Imaging, 660 First Ave, Fourth Floor, New York, NY 10016, USA. Email: faye.mckenna@nyulangone.org.

Abstract

Decreased brain lateralization is considered a trait marker of schizophrenia. Whereas reductions in both functional and macrostructural gray matter laterality in schizophrenia are well established, the investigation of gray matter microstructural lateralization has so far been limited to a small number of ex vivo studies, which limits the understanding of neurobiological substrates involved and development of adequate treatments. The aim of the current study was to assess in vivo gray matter microstructure lateralization patterns in schizophrenia by employing the diffusion kurtosis imaging (DKI)–derived mean kurtosis (MK) metric. MK was calculated for 18 right-handed males with chronic schizophrenia and 19 age-matched healthy control participants in 46 bilateral gray matter regions of interest (ROI). Microstructural laterality indexes (μLIs) were calculated for each subject and ROI, and group comparisons were conducted across regions. The relationship between μLI values and performance on the Wisconsin Card Sorting Test (WCST) was also evaluated. We found that compared with healthy controls, males with chronic schizophrenia had significantly decreased μLI across cortical and subcortical gray matter regions, which was correlated with poorer performance on the WCST. Our results suggest the ability of DKI-derived MK to capture gray matter microstructural lateralization pathology in vivo.

Key words: diffusion kurtosis imaging, executive function, gray matter, lateralization, schizophreniava

Introduction

One important characteristic of the healthy human brain is the lateralization of structure and function between the two hemispheres. Evolutionarily, lateralization exists in many vertebrate animals and is believed to be associated with increased neural capacity and reduced structure redundancy (Halpern 2005). Although the macrostructure of the two hemispheres appears nearly identical, at a microscopic level each hemisphere develops uniquely leading to lateralization. Some of the most defining asymmetry patterns in the healthy human brain lie in the leftward localization of brain regions involved in language, speech, and motor processing with increased left hemisphere volume, microstructural complexity, and functionality (Renteria 2012). Changes in cortical lateralization are a distinctive marker of several neurological diseases such as Alzheimer's disease, autism spectrum disorder, depression, and schizophrenia (SZ) (Hecht 2010; Renteria 2012; Sheng et al. 2013; Liu et al. 2018).

Whereas initial studies on cortical lateralization in SZ were conducted postmortem (Crow et al. 1989; Harrison 2000; Chance 2014), the advent of magnetic resonance imaging (MRI) has allowed for the in vivo study of lateralization. Recent studies have demonstrated the ability of multimodal neuroimaging to capture structural and functional asymmetries in the brain on

both the macroscopic and microscopic levels (Vernooij et al. 2007; Takao et al. 2010; Oertel-Knochel and Linden 2011; Alary et al. 2013; Sheng et al. 2013). Impaired macroscale structural lateralization of the gray matter (GM) in SZ has been well established through the use of T_1-weighted (T1w) anatomical MRI (Oertel et al. 2010; Takao et al. 2010; Okada et al. 2016). More recently, a growing body of functional MRI (fMRI) research has found both reduced lateralization of activated brain regions in language and listening tasks (Oertel et al. 2010; Alary et al. 2013) and impaired functional interhemispheric connectivity (Ribolsi et al. 2014; Zhang et al. 2018) in SZ. These fMRI findings suggest a plausible theory for the relationship between the altered structural and functional SZ asymmetry findings, where reduced lateralization of functionally specialized areas may result in altered inter- and intrahemispheric connections or vice versa. Although progress has been made in detailing lateralization abnormalities in SZ, the microstructural bases of these findings have not yet been investigated in vivo. Mapping of microstructural level changes may contribute critical information on the mechanisms that link structural deficits to abnormal connectivity and function.

Advances in diffusion MRI acquisition and postprocessing have led to the diffusion kurtosis imaging (DKI) technique proposed by Jensen et al. (2005), which allows the estimation of water diffusion non-Gaussianity through the mean kurtosis (MK) index. MK captures microstructural complexity that arises from the heterogeneous orientation, density, and organization of biological tissues (Jensen et al. 2005). DKI is particularly adept at imaging GM microstructure because of its sensitivity to diffusion variations in complex environments such as diversely oriented neurites in dendritic trees and axonal crossings (Jensen et al. 2005). Kurtosis, as the measurement of diffusion heterogeneity in the tissue, is thought to be more sensitive to pathology than standard DTI and therefore is a potential early biomarker of disease (Wang et al. 2011). Experiments by Das et al. (2017) reported that MK was the only diffusion parameter to show significant GM microstructural asymmetry in the healthy human brain in regions that were previously reported to have distinct lateralization on the macroscale level. As reported earlier, Lee et al. (2014) showed that DKI is superior to conventional DTI in detecting tract asymmetries in the healthy human brain, as DTI is only able to describe a single fiber orientation per voxel, which results in biases in the calculations of microstructural asymmetries. In this work, we use for the first time the MK metric to investigate in vivo lateralization of GM in SZ at the microstructural level. Diffusion techniques, including DKI, have to date predominantly focused on examining microscopic white-matter asymmetries in SZ (Park et al. 2004; Ribolsi et al. 2014). DKI is a robust method sensitive to a range of GM microscopic neuropathologies (Zhuo et al. 2012; Steven et al. 2014; Zhu et al. 2015), and therefore we expect that it may be instrumental in identifying SZ-specific lateralization patterns.

Impaired executive function is considered one of the SZ's most pronounced clinical features (Ilonen et al. 2000; Raffard and Bayard 2012). The Wisconsin Card Sorting Test (WCST) has been extensively used to test deficits in executive function in SZ (Ilonen et al. 2000), with neuroimaging studies correlating GM atrophy, gyrification abnormalities, hypofunction, and dysconnectivity in SZ to poor performance on this test (Ragland et al. 2007; Lee et al. 2013; Quan et al. 2013; Molina et al. 2017; Sasabayashi et al. 2017). Investigating the relationship between GM microscopic lateralization patterns measured by MK and performance on the WCST may offer additional insight into the biological bases of cognitive impairment in this disorder.

In summary, the aim of this work is to characterize differences in microstructural lateralization of cortical and subcortical GM in chronic SZ patients versus healthy control (HC) participants. We also hypothesize that altered GM microstructure lateralization in SZ is associated with poor WCST performance, consistent with the assumption that healthy lateralization promotes neural capacity and efficiency.

Methods and Materials

Participants

Male individuals with SZ ($n = 18$) and matched HCs ($n = 19$) were recruited by referral from clinicians at New York City's Bellevue Hospital and by advertisement (Table 1). Patients were interviewed by a licensed clinical psychologist and administered the Structured Clinical Interview for DSM-IV (SCID-IV) for Axis-I disorders patient edition (Spitzer et al. 1994). The nonpatient edition of the SCID-IV was administered to HC participants to confirm the lack of a psychiatric diagnosis. The SZ group included individuals with either SZ ($n = 17$) or schizoaffective disorder ($n = 1$). All participants were right-handed males, aged 30–55 years old. Participants were excluded for substance abuse within the last 6 months, head trauma with loss of consciousness for more than 30 minutes, or presence of other neurological disorders. Socioeconomic Status (SES) scores were obtained for all participants and their parents based on the Hollingshead scale (Hollingshead 2011). The study was approved by institutional review boards at New York University School of Medicine and Bellevue Hospital.

Magnetic Resonance Image Acquisition

All MRI data was acquired on a 3T Trio MRI (Siemens Medical Solutions, Erlangen, Germany) at the Center for Biomedical Imaging, Department of Radiology, New York University School of Medicine between 2010 and 2012. Study participants were scanned in the order they were recruited, with recruitment and assessment following an alternating pattern of four to five patients followed by four to five HC participants. All participants were scanned under the same protocol with no MRI scanner upgrades taking place during the study. A T1w MPRAGE image was collected using the standard high-resolution product Siemens protocol employing a voxel size of $1 \times 1 \times 1$ mm^3. Diffusion imaging data was acquired using a diffusion-weighted spin echo planar imaging (EPI) sequence for a total of 64 uniformly distributed gradient directions and for two b values ($b = 1000$ and 2000 s/mm^2). Ten non-weighted diffusion images ($b = 0$ s/mm^2) were also collected. Fifty-five slices with a slice thickness of 2.3 mm were collected to obtain approximate whole brain coverage. An in-plane resolution of 2.3×2.3 mm was employed resulting in an isotropic voxel for the diffusion images. In addition, a field map image coplanar to the diffusion acquisition was acquired using a pair of non-EPI gradient echo images at two echo times and employed to correct for image distortions from B0 field inhomogeneities.

MK maps were calculated using in-house developed software and FSL suite (Jenkinson et al. 2012). All data preprocessing included the following: 1) visual inspection of images for quality assessment and absence of artifacts, 2) coregistration of diffusion images using FSL Flirt, 3) correction for B0 field

Table 1 Demographic and clinical characteristics of the participants

	SZ ($n = 18$), mean ± SD	Healthy control ($n = 19$), mean ± SD	*t*-test *P*-value
Male/female	18/0	19/0	—
African American	9	6	—
Caucasian	5	10	—
Other	4	3	—
Hispanic/non-Hispanic	4/14	2/17	—
Age (years)	45 ± 6	42 ± 6	0.427
Handedness (right/left)	18/0	19/0	—
Educations (years)	12.6 ± 2.3	15.7 ± 1.8	<0.001
SES participants (score)	1.9 ± 4	4.5 ± 1.3	<0.001
SES parents (score)	3.8 ± 1.7	4.6 ± 1.5	0.058
Perseverative Errors	25.5 ± 20.7	9.6 ± 8.1	0.004
Total Errors	49.25 ± 28.2	18.68 ± 14.9	<0.001
Conceptual Level Response	50.3 ± 22.6	66.8 ± 8.9	0.006
Categories Completed	3.9 ± 2.6	5.8 ± 0.6	0.001

Note: SD = standard deviation.

inhomogeneities distortion using the acquired field map data and FSL, and 4) image smoothing using a 3D Gaussian filter with $\sigma = 1.4$ mm. After data correction, diffusion and kurtosis tensors were calculated as previously described by Tabesh et al. (2011). The effect of image rotation from the motion correction step was compensated for by adjusting the encoding gradients' matrix (Leemans and Jones 2009). The kurtosis tensors were employed to derive 3D maps of MK.

Image Processing

FreeSurfer software (http://surfer.nmr.mgh.harvard.edu/) was used to construct the cortical surface of each participant based on the high-resolution T1w image. The FreeSurfer pipeline for surface construction, described in more detail by Fischl and Dale (2000), includes segmentation based on tissue types, tessellation of the GM/white matter junction, inflation of the folded surface, and parcellation using the Desikan–Killiany atlas (Desikan et al. 2006). Cortical thickness metrics were also obtained for the 4 GM lobes and 68 bilateral GM regions of interest (ROIs) and employed to test whether MK changes relate to variations in macrostructure. The resulting subject-specific cortically labeled volumes were then transformed into the diffusion MRI space of each subject using FreeSurfer's rigid-body transformation (Fischl and Dale 2000). Mean MK of the four bilateral cortical lobes (frontal, parietal, temporal, and occipital) and 68 bilateral cortical and 16 subcortical ROIs (i.e., 42 regions in each hemisphere) were extracted for each subject in the anatomically parcellated diffusion space. Previous research has suggested good within-subject repeatability of FreeSurfer with a capital's anatomical parcellation even for smaller subcortical ROIs (Wonderlick et al. 2009; Jovicich et al. 2013). Visual assessment of each data set was used to confirm a good quality of both parcellation and its registration onto the diffusion space.

The microstructural laterality index (μLI) of each region was subsequently calculated using the equation ($\mu LI = [L-R]/[L+R]$), where L represents the mean MK of voxels in the left-hemisphere ROI or lobe, and R represents the mean MK of voxels in the right-hemisphere ROI or lobe. Positive values of μLI ranging from greater than 0 to 1 indicate that MK is greater in the left-hemisphere ROI, negative values of μLI ranging from less than 0 to −1 indicate that MK is greater in the right-hemisphere ROI, and a value of 0 indicates no differences in MK between left and right hemisphere ROIs. The pattern of GM microstructural lateralization in each participant is therefore established by the direction, or lack of direction, of the μLI of each GM ROI. On the individual and/or group level, the degree that μLI deviates in SZ from HC in each ROI may indicate how SZ pathology affects GM lateralization.

In addition, for each SZ participant, we derived a laterality deviation index (LDI) defined by the absolute difference of individual μLI and the average HC μLI for each ROI.

Cognitive Testing

The WCST was administered by a licensed clinical psychologist. The following scores were recorded and analyzed: Categories Completed, Conceptual Level Response, Perseverative Errors, and Total Errors. The WCST assesses a range of cognitive functions by requiring participants to sort cards by a series of principles they must deduce based on stimuli printed on a set of cards: shape, color, and number. There is an arbitrary correct sorting principle that participants learn solely through tester feedback of right and wrong, and this principle changes every 10 consecutive trials for up to six category trials.

Statistical Analyses

Primary analyses evaluated between-group differences (i.e., SZ vs. HC) in the μLI using independent-samples student *t*-tests. Nonparametric Mann–Whitney U tests were also used to confirm *t*-tests results. ROIs included the four bilateral cortical lobes (frontal, parietal, temporal, and occipital) and 42 bilateral cortical and subcortical regions. Controlling for the effects of age and education using Analysis of Covariance (ANCOVA) with either age or education as the covariate had no major effects on the between-group comparisons (Supplementary Table 1). Cohen's d effect size was calculated to compare group means for each ROI analysis. Power estimates were additionally calculated for *t*-tests to detect observed differences using the observed standard deviations at $P \leq 0.001$ (0.05/46) Bonferroni corrected significance level using PASS 11 software (Number Cruncher Statistical Systems, Kaysville, UT, 2011).

Additional analyses assessed associations between WCST scores (Categories Completed, Conceptual Level Response,

Table 2 Microstructural lateralization index differences in SZ compared with HC in the GM lobes

Region	Mean μLI	SD	Mean μLI	SD	Mean difference from HC	t-test P-value	Mann–Whitney U P-value	Cohen's d	Power
	SZ		HC						
Frontal lobe	−0.005	+/−0.017	0.054	+/−0.028	−0.059	<0.001*	<0.001*	0.848	0.99
Parietal lobe	0.005	+/−0.013	0.028	+/−0.019	−0.014	<0.001*	<0.001*	0.453	0.75
Temporal lobe	0.003	+/−0.025	−0.067	+/−0.029	0.026	<0.001*	<0.001*	0.861	0.99
Occipital lobe	−0.008	+/−0.044	0.012	+/−0.015	−0.190	0.079	0.075	0.191	0.05

Note: μLI of cortical GM lobes in SZ versus HCs. The μLI measures the hemispheric lateralization of DKI-derived MK; positive μLI indicated leftward asymmetry, and negative μLI indicated rightward asymmetry. Significant differences between groups (*$P \leq 0.001$) are noted across regions along with the effect size (Cohen's d) and the power of the difference between groups.

Perseverative Errors, and Total Errors subcategories) and LDI for each SZ participant using Pearson's and Spearman's rank correlations. Pearson's and Spearman's correlations were both calculated because the discrepancy between them is informative in describing the true relationship between the diffusion metrics and cognitive performance.

The GM cortex is thinner in SZ compared with HC, and therefore between–group differences in MK and μLI may be driven by partial volume averaging and differences at macrostructural level. To test if MK values are affected by partial volume averaging, we conducted Pearson's correlation analysis of cortical thickness measures with MK values for each cortical lobe and ROI on a per-subject basis in SZ and HC groups separately (Supplementary Table 2).

To account for multiple comparisons across the 42 cortical and subcortical regions and four cortical lobes, we employed Bonferroni correction. Thus, to achieve a family-wise type I error rate ≤0.05 (two-sided), individual results were considered significant for $P < 0.05/46$, which is met if $P \leq 0.001$. Differences with $P < 0.05$ were considered to reach trend level.

Results

Participants

Demographic information for both groups is presented in Table 1. The groups were perfectly matched in terms of gender and handedness since all participants were right-hand males. No significant between-group differences were noted in age and parental SES. As expected, patients had significantly fewer education years and significantly poorer performance on the WCST (Table 1).

Lobar Brain Differences in Microstructural Laterality

Frontal, temporal, and parietal laterality was significantly different in the SZ versus HC groups ($P \leq 0.001$), with SZ showing an overall pattern of reduced μLI (Table 2). In HC participants, leftward lateralization was noted in frontal and parietal lobes and rightward for the temporal lobe, while SZ participants showed significantly reduced hemispherical asymmetry (Table 2).

Cortical Differences in Microstructural Laterality

The laterality index was significantly different in SZ compared with HC participants in multiple cortical regions including the banks of the superior temporal sulcus, pars opercularis division of inferior frontal gyrus, caudal and rostral middle frontal, inferior temporal, lingual, parahippocampal, precentral, superior temporal and supramarginal gyri, insula, lateral and medial orbitofrontal, precuneus, superior parietal and transverse temporal cortices, isthmus, posterior and rostral anterior divisions of the cingulate cortex, paracentral lobule, and temporal pole ($P \leq 0.001$) (Table 3; Figs 1 and 2).

Notably, every cortical region that showed significantly different μLI in SZ, with the exception of the caudal anterior cingulate cortex, had markedly decreased bilateral asymmetry (Table 3; Fig. 1). The cortical regions that showed the greatest difference in laterality in SZ versus HC were the banks of the superior temporal, precentral, rostral middle frontal, superior and inferior temporal gyri, and temporal pole (Table 3).

Figure 2 highlights that in HCs, areas of similar laterality correspond to well-defined brain networks (i.e., prefronto-parietal and orbitofrontal-cingulate-temporal networks). More specifically, we note a leftward lateralization of regions involved in language (the banks of the superior temporal sulcus, supramarginal and pars opercularis areas) and motor (precentral) functions, matching functional lateralization patterns established in the field. Despite the significantly reduced laterality in the SZ group, a reverse trend in lateralization (e.g., rightward vs. leftward; rightward vs. leftward) is apparent (Fig. 2).

Subcortical Differences in Microstructural Laterality

Similar to the cortical ROIs, subcortical ROIs showed substantially less lateralization ($P \leq 0.001$) between the right and left hemispheres in SZ versus HC participants in all structures but the putamen, for which differences were observed at trend level (Table 4; Fig. 3). The greatest difference in lateralization between SZ and HC participants was found in the pallidum (mean LDI = 0.191 $\pm 0.029, d = 1.287$), nucleus accumbens (mean LDI = −0.121 $\pm 0.019, d = 0.711$), thalamus proper (mean LDI = 0.113 $\pm 0.005, d = 1.282$), and ventral diencephalon (mean LDI = 0.114 $\pm 0.006, d = 1.718$) (Table 4; Figs 3 and 4). Figure 4 shows the complete separation between groups in terms of the μLI of these three structures, with the minimum μLI value of each structure among individuals with SZ being higher than the maximum value among HCs. This implies that the μLI of these three structures achieved 100% accuracy for the discrimination of the SZ and HC groups in our sample.

Association Between Cognitive Metrics and LDI in SZ

Significant Pearson's correlations ($P \leq 0.001$) were observed between increased LDI in SZ and poor performance on three

Table 3 Microstructural Lateralization Index Differences in SZ Compared to HC in Cortical GM ROIs

	Region	Mean μLI	SD	Mean μLI	SD	Mean difference from HC	*t*-test *P*-value	Mann–Whitney U *P*-value	Cohen's d	Power
Frontal Lobe		SZ		HC						
	Caudal middle frontal	−0.005	+/−0.021	0.066	+/−0.024	−0.072	<0.001**	<0.001**	1.028	0.99
	Frontal pole	−0.004	+/−0.034	0.024	+/−0.041	−0.028	0.034*	0.068	0.245	0.12
	Lateral orbital frontal	0.012	+/−0.032	−0.042	+/−0.020	0.054	<0.001**	<0.001**	0.662	0.98
	Medial orbital frontal	0.006	+/−0.021	−0.055	+/−0.033	0.062	<0.001**	<0.001**	0.721	0.99
	Paracentral	0.008	+/−0.032	−0.025	+/−0.017	0.033	<0.001**	<0.001**	0.425	0.58
	Pars orbitalis	0.000	+/−0.064	−0.026	+/−0.022	0.026	0.100	0.081	0.183	0.03
	Pars opercularis	−0.005	+/−0.024	0.060	+/−0.022	−0.065	<0.001**	<0.001**	0.914	0.99
	Pars triangularis	−0.011	+/−0.035	0.007	+/−0.016	−0.018	0.051	0.004*	0.218	0.07
	Precentral	−0.004	+/−0.015	0.123	+/−0.081	−0.127	<0.001**	<0.001**	0.728	0.99
	Superior frontal	0.002	+/−0.019	0.021	+/−0.028	−0.018	0.024*	0.013*	0.256	0.15
	Rostral middle frontal	−0.011	+/−0.019	0.112	+/−0.043	−0.123	<0.001**	<0.001**	1.231	0.99
Parietal Lobe	Inferior parietal	0.007	+/−0.028	0.035	+/−0.022	−0.027	0.003*	0.001**	0.349	0.43
	Postcentral	0.007	+/−0.016	0.020	+/−0.019	−0.013	0.035*	0.039*	0.238	0.12
	Precuneus	0.007	+/−0.017	−0.050	+/−0.026	0.058	<0.001**	<0.001**	0.846	0.99
	Supramarginal	−0.001	+/−0.019	0.052	+/−0.056	−0.054	0.001**	<0.001**	0.424	0.56
	Superior parietal	0.005	+/−0.017	0.065	+/−0.029	−0.059	<0.001**	<0.001**	0.800	0.99
Temporal Lobe	Bankssts	−0.003	+/−0.038	0.093	+/−0.033	−0.096	<0.001**	<0.001**	0.876	0.99
	Entorhinal	−0.027	+/−0.038	−0.050	+/−0.071	0.023	0.232	0.425	0.132	0.02
	Fusiform	0.008	+/−0.035	−0.039	+/−0.068	0.047	0.012*	0.057	0.285	0.19
	Inferior temporal	0.017	+/−0.056	−0.105	+/−0.049	0.123	<0.001**	<0.001**	0.766	0.99
	Parahippocampal	−0.13	+/−0.030	−0.059	+/−0.032	0.045	<0.001**	<.001**	0.476	0.81
	Middle temporal	0.004	+/−0.029	−0.020	+/−0.030	0.024	0.018*	0.026*	0.268	0.16
	Superior temporal	−0.003	+/−0.013	−0.131	+/−0.050	0.128	<0.001**	<.001**	1.160	0.99
	Temporal pole	−0.001	+/−0.033	−0.124	+/−0.077	0.122	<0.001**	<.001**	0.682	0.99
	Transverse temporal	0.002	+/−.015	−0.073	+/−0.031	0.075	<0.001**	<.001**	1.015	0.99
Occipital Lobe	Cuneus	−0.002	+/−0.026	0.020	+/−0.034	−0.022	0.030*	0.020*	0.241	0.11
	Lateral occipital	0.003	+/−0.063	0.018	+/−0.044	−0.014	0.430	0.461	0.086	0.01
	Lingual	0.000	+/−0.030	−0.046	+/−0.020	0.046	<0.001**	<0.001**	0.592	0.95
	Pericalcarine	0.009	+/−0.044	0.023	+/−0.012	−0.013	0.202	0.007*	0.141	0.16
Other	Caudal anterior cingulate	0.011	+/−0.021	−0.010	+/−0.027	0.021	0.012*	0.026*	0.287	0.20
	Insula	−0.007	+/−0.016	0.028	+/−0.034	0.036	<0.001**	<0.001**	0.435	0.63
	Isthmus cingulate	0.006	+/−0.034	−0.048	+/−0.019	0.054	<0.001**	<0.001**	0.644	0.98
	Posterior cingulate	0.008	+/−0.016	−0.017	+/−0.021	0.025	<0.001**	<0.001**	0.431	0.69
	Rostral anterior cingulate	0.014	+/−0.027	0.071	+/−0.056	−0.056	<0.001**	<0.001**	0.425	0.61

Note: μLI of cortical GM ROIs in SZ versus HCs. The μLI measures the hemispheric lateralization of DKI-derived MK; positive μLI indicated leftward asymmetry, and negative μLI indicated rightward asymmetry. Significant *p <.05 differences between groups (**$P \leq 0.001$) are noted across regions along with the effect size (Cohen's d) and the power of the difference between groups.

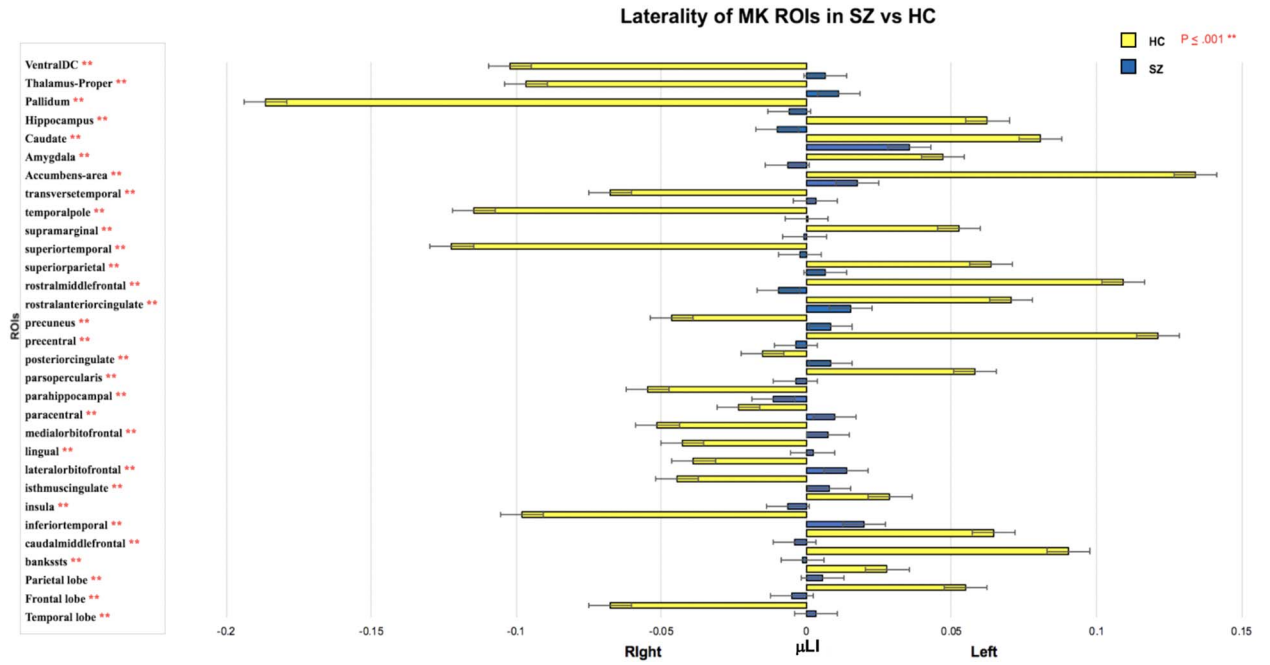

Figure 1. The μLI across cortical and subcortical regions in SZ compared with HC. Rightward, positive value, bars indicate left lateralization and leftward, negative value, bars indicate right lateralization with error bars indicating standard deviation in the group. Data shown for regions with significant between group differences in μLI (**$P \leq 0.001$).

Table 4 Microstructural lateralization index differences in SZ compared with HC in subcortical GM ROIs

Region	Mean μLI	SD	Mean μLI	SD	Mean difference from HC	t-test P-value	Mann–Whitney U P-value	Cohen's d	Power
	SZ		HC						
Accumbens	0.016	+/−0.045	0.137	+/−0.064	−0.121	<0.001**	<0.001**	0.711	0.99
Amygdala	−0.008	+/−0.032	0.046	+/−0.050	−0.055	<0.001**	<0.001**	0.430	0.62
Caudate	0.036	+/−0.029	0.083	+/−0.026	−0.047	<0.001**	<0.001**	0.556	0.93
Hippocampus	−0.011	+/−0.012	.064	+/−0.029	−0.074	<0.001**	<0.001**	1.098	0.99
Pallidum	−0.008	+/−0.032	−0.199	+/−0.061	0.191	<0.001**	<0.001**	1.287	0.99
Putamen	−0.001	+/−0.032	0.053	+/−0.065	−0.055	0.003*	0.019*	0.352	0.35
Thalamus proper	0.010	+/−0.026	−0.103	+/−0.031	0.113	<0.001**	<0.001**	1.282	0.99
Ventral diencephalon	0.005	+/−0.018	−0.108	+/−0.024	0.114	<0.001**	<0.001**	1.718	0.99

Note: μLI of cortical GM ROIs in SZ versus HCs. The μLI measures the hemispheric lateralization of DKI-derived MK with positive μLI indicating leftward asymmetry and negative μLI rightward asymmetry. Significant differences between groups (**$P \leq 0.001$) and differences at trend level (*$P < 0.05$) are noted across regions along with the effect size (Cohen's d) and power of the difference between groups.

of the four WCST scores: Categories Completed, Conceptual Level Response, and Perseverative Errors with relationship with total errors reaching trend levels (Table 5; Fig. 5). A lower score on the Categories Completed and Conceptual Level Response subcategories was indicative of poor cognitive function and test performance. The WCST Categories Completed and Conceptual Level Response subcategories were therefore negatively correlated to LDI (Table 5; Fig. 5). A higher score on the Perseverative Errors and Total Errors was indicative of poor cognitive function and test performance and was therefore positively correlated to LDI (Table 5; Fig. 5). A good correspondence was generally found between Pearson's and Spearman's correlation results with some discrepancies noted for μLI associations with Perseverative Errors, where Pearson's correlations were in part driven by the presence of one to two participants with high LDI and very poor performance on the test.

Association Between Cortical Thickness and MK Values

No significant correlations ($P \geq 0.001$) were observed between T1w cortical thickness metrics and MK values in the 4 lobes and 68 cortical ROIs in either SZ or HC groups (Supplementary Table 2). Only 8 of the 72 GM ROIs tested reached trend-level association at $P < 0.05$ (Supplementary Table 2). These results suggest that cortical MK values are likely unbiased by partial volume averaging.

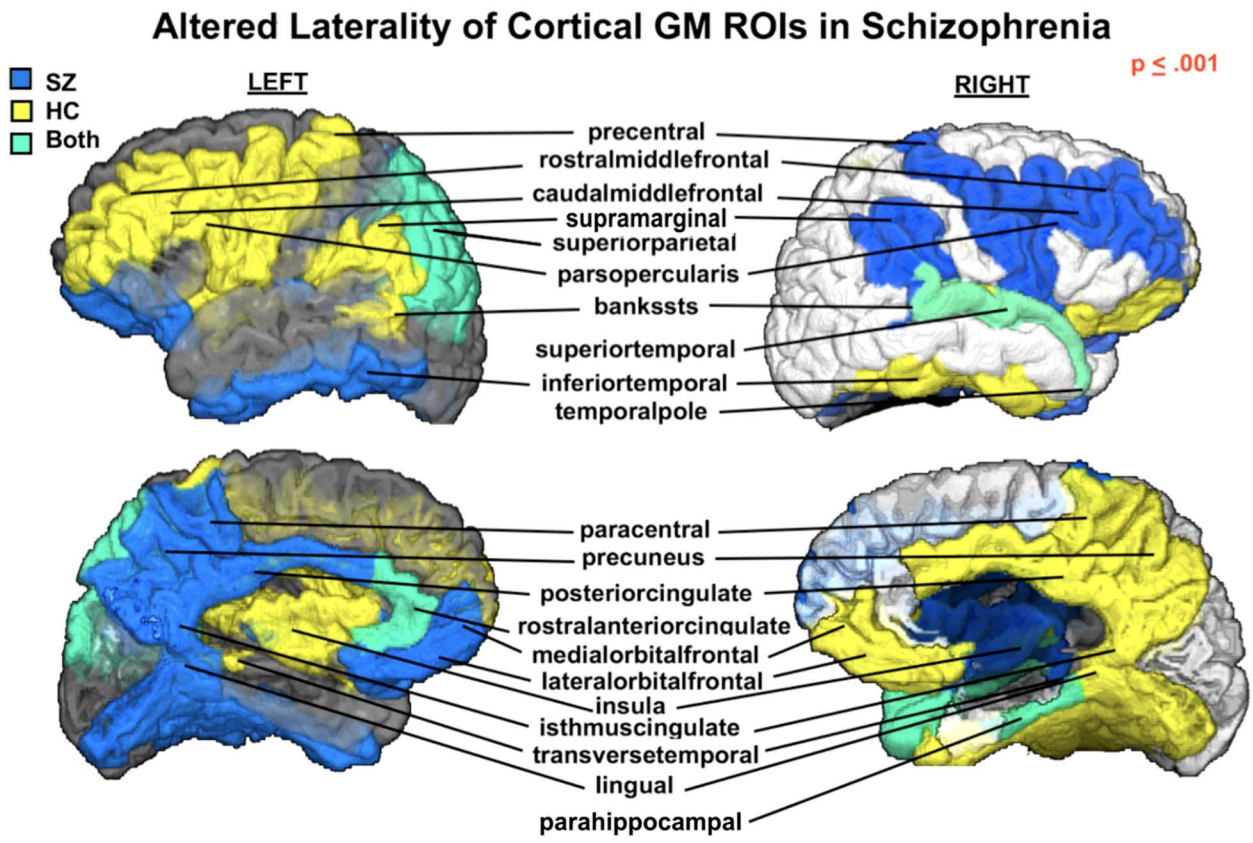

Figure 2. Cortical laterality (left vs. right) displayed for regions with significantly different μLI ($P \leq 0.001$) in SZ compared with HCs. Color indicates group (SZ—blue, HC—yellow, SZ&HC—green) μLI direction for each ROI. In the HC group, the fronto-parietal motor and language areas appear left lateralized, whereas the orbitofrontal-cingulate-temporal areas are right lateralized. These lateralization patterns are largely lost in SZ (see Figure 1) with a reversed trend (right vs. left or left vs. right) observed.

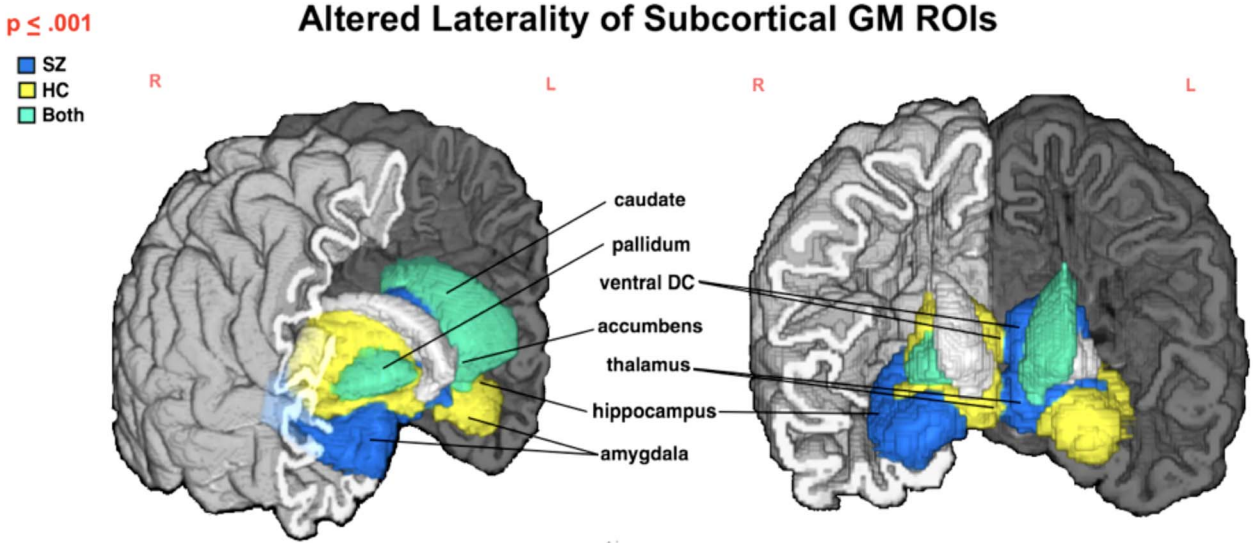

Figure 3. Subcortical structures with significantly different μLI ($P \leq 0.001$) in SZ compared with HC. Color indicates group (SZ—blue, HC—yellow, SZ&HC—green) μLI direction for each ROI. In HC, amygdala, caudate, hippocampus, and nucleus accumbens are left lateralized with thalamus, pallidum and ventral diencephalon being right lateralized. Both a decrease in lateralization (see Table 4; Figure 3) and a reversed trend (i.e., right vs. left lateralization or left vs. right) are noted in SZ for several structures.

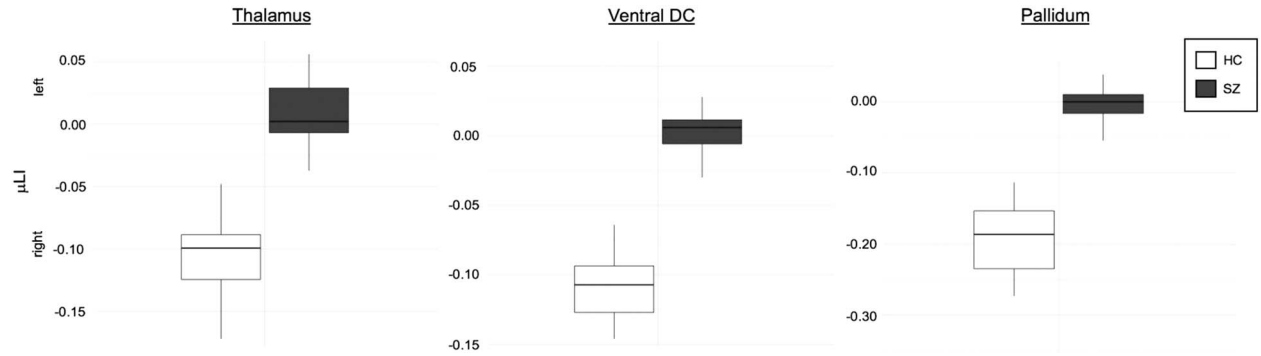

Figure 4. The three subcortical structures with complete separation of HC and SZ groups' μLI. Color indicates group (SZ—gray, HC—white) for each ROI: thalamus, ventral diencephalon (ventral DC) and pallidum. HC had rightward lateralization in ROIs, while SZ had significantly decreased ($P \leq 0.001$) asymmetry.

Table 5 Correlation between LDI and WCST scores in SZ

WCST measure	Region	Pearson's r	Pearson's *P*-value	Spearman's r_s	Spearman's *P*-value
Categories Completed	Pars opercularis	−0.52	0.040*	−0.47	0.067
	Medial orbital frontal	−0.55	0.026*	−0.19	0.480
	Rostral anterior cingulate	−0.65	0.006*	−0.53	0.035*
	Rostral middle frontal	−0.54	0.029*	−0.43	0.094
	Accumbens	−0.76	0.001**	−0.72	0.002*
	Amygdala	−0.80	<0.001**	−0.56	0.023*
Concept Level Response	Caudal middle frontal	−0.56	0.025*	−0.46	0.073
	Insula	−0.59	0.017*	−0.34	0.195
	Medial orbital frontal	−0.58	0.019*	−0.24	0.373
	Parahippocampal	−0.40	0.122	−0.64	0.007*
	Pars opercularis	−0.75	0.001**	−0.63	0.009*
	Precentral	−0.56	0.023*	−0.42	0.103
	Precuneus	−0.53	0.036*	−0.42	0.104
	Rostral anterior cingulate	−0.70	0.002*	−0.61	0.010*
	Rostral middle frontal	−0.61	0.013*	−0.54	0.032*
	Superior frontal	−0.54	0.030*	−0.23	0.382
	Superior temporal	−0.51	0.044*	−0.36	0.171
	Transverse temporal	−0.51	0.043*	−0.40	0.129
	Accumbens	−0.75	0.001**	−0.67	0.005*
	Amygdala	−0.69	0.003*	−0.60	0.014*
Perseverative Errors	Caudal middle frontal	0.57	0.021*	0.43	0.097
	Insula	0.55	0.027*	0.12	0.658
	Lateral orbital frontal	0.73	0.001**	0.04	0.871
	Pars opercularis	0.78	<0.001**	0.45	0.083
	Pars orbitalis	0.69	0.003*	0.02	0.931
	Pars triangularis	0.55	0.028*	0.28	0.295
	Superior frontal	0.67	0.004*	0.43	0.097
	Supramarginal	0.54	0.032*	0.13	0.633
Total Errors	Entorhinal	0.50	0.048*	0.52	0.048*
	Parahippocampal	0.21	0.433	0.53	0.033*
	Pars opercularis	0.63	0.010*	0.56	0.024*
	Rostral anterior cingulate	0.51	0.045*	0.44	0.087
	Accumbens	0.69	0.003*	0.68	0.004*
	Amygdala	0.59	0.015*	0.55	0.028*

Note: Correlation between LDI and WCST scores in the SZ group. LDI is measured as the absolute difference of μLI values for SZ patients and mean μLI of the HC group. Regions with significant LDI associations with WCST scores (**$P \leq 0.001$) and those associated at trend level (*$P < 0.05$) are included in the table.

Discussion

MK Laterality Abnormalities in SZ

Neuroimaging studies have documented functional and macrostructural GM lateralization abnormalities in SZ using T1w MRI, fMRI, Positron Emission Tomography (PET), and Single-Photon Emission Computerized Tomography (SPECT) techniques (Russell et al. 1997; Artiges et al. 2000; Takao et al. 2010; Oertel-Knöchel and Linden 2011; Sheng et al. 2013; Royer et al. 2015; Okada et al. 2016). However, to date, the investigation of the asymmetry in cytoarchitectural and microstructural GM features has been limited to postmortem analyses (Harrison

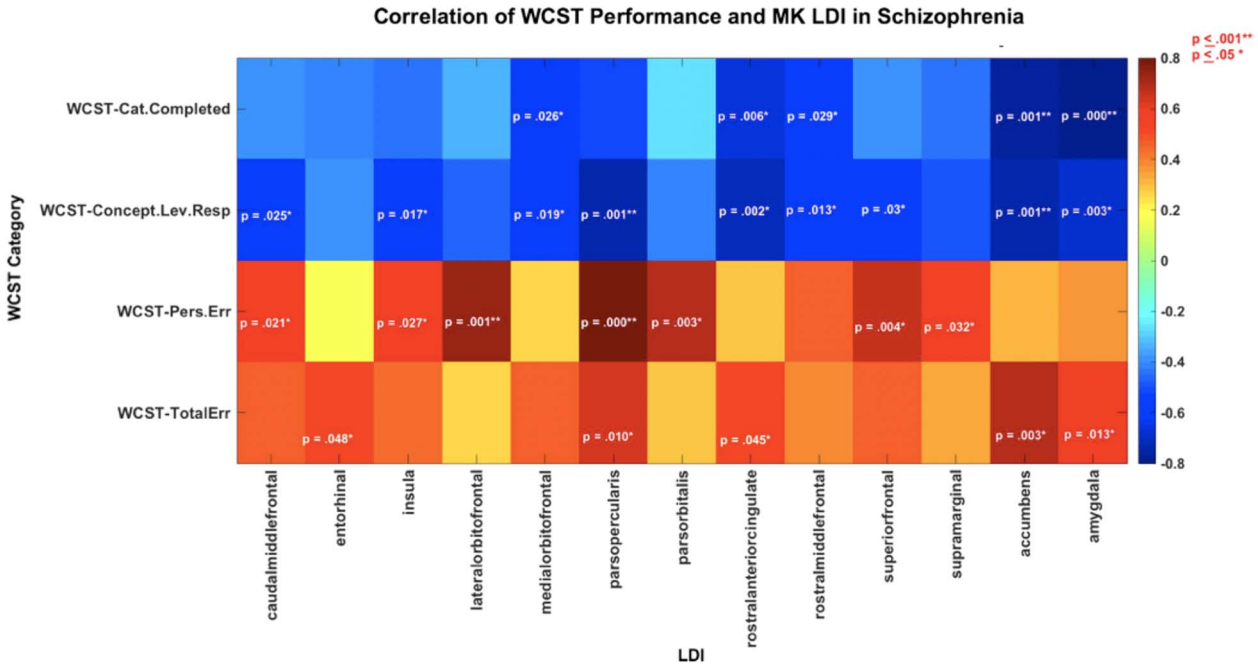

Figure 5. Graphical representation of the associations between LDI and performance on four subcategories of the WCST in the SZ group. For the Categories Completed and Concept Level Response, subcategories of the WCST a higher score indicated better performance, whereas for the Perseverative Error and Total Error, subcategories of the WCST a lower score indicated a better performance. Higher LDI in SZ associated with poorer performance on the WCST. Significant ($**P \leq 0.001$) and trend level associations ($*P \leq 0.05$) are noted by the listed *P-values*; the strength of the correlation (i.e., Pearson's *r* value) is represented using the associated color map.

2000; Hutsler and Galuske 2003; Cullen et al. 2006; Steiner et al. 2006; Chance et al. 2008; Di Rosa et al. 2009; Chance 2014). To the best of our knowledge, this is the first in vivo study that investigates GM microstructural asymmetry deficits in SZ using diffusion imaging. Our results suggest that SZ is associated with significantly decreased microstructural lateralization of several subcortical and cortical structures. Our findings also highlight that MK, an in vivo metric of tissue microstructural complexity, may be informative in describing GM microarchitectural lateralization.

In the HC group, leftward GM MK lateralization was observed primarily in regions of the frontal and parietal lobes, with orbitofrontal, cingulate, and inferior temporal areas being right lateralized (Fig. 2). Thus, in language, face processing, and motor regions, which are known to be functionally lateralized, increased kurtosis appears to characterize the dominant hemisphere (i.e., left for the lateral prefrontal, banks of the superior temporal sulcus, supramarginal gyrus, and precentral cortex regions and right for the fusiform gyrus). Histological studies have shown that dominant language areas are characterized by larger neuronal bodies (Hutsler and Galuske 2003), wider cortical minicolumns (Chance et al. 2008), and axons that are more thickly myelinated (Anderson et al. 1999) compared with their contralateral sides. It has been suggested that these axons may better support long range connectivity and function, resulting in these areas' well-known lateralization (Geschwind and Levitsky 1968; Anderson et al. 1999; Chance 2014). Thus, we hypothesize that increased kurtosis in the dominant language areas of the healthy brain may arise from a larger number of more thickly myelinated connections that descend into deep white matter regions. The GM kurtosis modulation by myelination has been recently highlighted by cuprizone demyelination studies in mice (Guglielmetti et al. 2016), which showed not only that cortical kurtosis decreases with demyelination but also that myelination changes may have a dominant effect on cortical kurtosis measurements. Microstructural lateralization in face processing areas in this study's HC group also appears to parallel the known rightward functional dominance. The cerebral asymmetries noted in the HC group using MK are highly consistent with a recent report that employed a model-driven diffusion imaging technique, the neurite orientation dispersion, and density (NODDI) (Schmitz et al. 2019).

Compared with the HC group, SZ participants had a significantly decreased lateralization index in a number of cortical GM regions (Table 3). These regions included areas known to be involved in language (pars opercularis, transverse temporal cortex, supramarginal gyrus, banks of the superior temporal sulcus), motor (precentral gyrus, paracentral lobule), sensory (postcentral gyrus), memory (inferior temporal, parahippocampal and superior frontal gyri), face processing (fusiform gyrus), executive control (rostral anterior cingulate cortex, frontal pole, lateral and medial orbital frontal cortices), and emotion (insula, inferior parietal, and posterior cingulate cortices) functions. Robust between-group differences were also found in MK lateralization of subcortical structures. Decreased lateralization of these areas may reflect a loss of functional specialization in SZ and may relate to the known impairments across multiple functional domains which characterize the disorder.

Our previous work has shown that MK in GM is increased in chronic SZ compared with HC participants (Lazar et al., 2015; Lazar et al., 2017). This increase was hypothesized to have several potential causes, including differences in neuronal density and/or neuronal organization and inflammation. In the healthy brain, increased kurtosis is associated with brain

maturation and improved cognitive functioning (Helpern et al. 2011; Bester et al. 2015). Given that in SZ MK's relationship to cognitive function appears to follow the same pattern as in HCs (increased kurtosis associated with better function) (McKenna et al. 2018), we further hypothesized that the observed kurtosis increase in SZ may reflect a layered effect of pathology on top of typical microstructural organization. The reduced asymmetry observed here appears to be related to increased kurtosis occurring more prominently in the typically nondominant hemisphere (Fig. 6). Considering the existing body of literature, we hypothesize that the observed bilateral pattern of change in SZ is likely the effect of the following additive phenomena: 1) a reduction of the healthy microstructural asymmetry due to reduced neuropil in the typically dominant hemisphere caused by less myelinated axons and/or reduced or atrophied dendrites and 2) an overall bilateral increase in microstructural complexity caused by pathological processes known to be associated with increased kurtosis and documented in SZ ex vivo such as activated/swollen astrocytes or microglia and increased neuronal or glial packing. This hypothesis aligns with both a long-standing hypothesis in the field, the reduced neuropil/increased neuronal density hypothesis (Selemon and Goldman-Rakic 1999), and current findings of reduced myelin in both GM (Tishler et al. 2018) and white matter (Scheel et al. 2013; Lazar et al. 2015). The neuropil, which borders cortical neuronal minicolumns, contains both local (dendrites) and long distance (axons) neuronal processes. Aberrations in neuropil may result in both reduced intracortical myelin and less myelinated long-distance connections along with abnormal white matter, which has been extensively documented through diffusion tensor imaging in SZ and proposed to be due to dysmyelination (Scheel et al. 2013; Lazar et al. 2015). Alternatively, smaller but more numerous minicolumns (Chance et al. 2008) and/or increased neuronal and glial density occurring more prominently in the nondominant hemispheres may also provide a possible but less likely explanation of the results here. Several studies have reported increased neuronal packing in SZ patients (Selemon et al. 1995; Selemon and Goldman-Rakic 1999; Casanova et al. 2008; Chance et al. 2008) and astrocyte swelling (Uranova et al. 2011), although they did not discriminate between right and left hemispheres. Future multimodal imaging studies will be essential to providing additional information needed to discriminate among these different possible pathological mechanisms of SZ.

Research documenting microstructural lateralization abnormalities in SZ remains limited to few brain regions and ex vivo studies. Chance et al. (2008) found that alterations in minicolumn spacing most contributed to reduced total volume asymmetry in the superior temporal gyrus in SZ. Di Rosa et al. (2009) documented absent or reversed asymmetry of fusiform pyramidal cell density in men with SZ, and Steiner et al. (2006) found that SZ patients had an absence of rightward lateralized cerebral microglial cells in the dorsolateral prefrontal cortex, normally present in healthy individuals. Few studies have concentrated on changes in symmetry of subcortical GM regions in SZ (Harrison 2000; Byne et al. 2002; Steiner et al. 2006). Steiner et al. (2006) found reduced lateralization of microglia cell density in the hippocampus postmortem. At macroscale level, Okada et al. (2016) found reduced yet leftward lateralization in the thalamus and ventral diencephalon similar to that indicated by our data. More integrative approaches to studying the macro and microstructural cortical deficits in SZ, combining postmortem and in vivo MRI techniques, will be instrumental in piecing together the relationship between the documented cortical and subcortical changes, axonal pathway alterations, and functional deficits.

MK Laterality Abnormalities and Cognition

Several studies have previously shown that individuals with SZ perform poorly on the WCST, and furthermore, that this altered cognitive function is linked to abnormalities in frontal lobe structures measured by fMRI, PET, T1w MRI, and DTI tractography (Kawasaki et al. 1993; Riehemann et al. 2001; Rüsch et al. 2007; Lee et al. 2013). Consistent with these findings, our analyses show associations between WCST domains and LDI of several frontal lobe regions. Significant associations were observed between increased Perseverative Errors and increased LDI in the lateral orbital frontal and pars opercularis GM ROIs in SZ, and between decreased WCST Conceptual Level Responses and increased LDI in the pars opercularis (Fig. 5; Table 5) with additional associations noted at trend level. Furthermore, WCST subtests correlated with the LDI of several ROIs involved in emotion, memory, and reward: entorhinal cortex, insula, rostral anterior cingulate cortex, supramarginal gyrus, accumbens, and amygdala ROIs (Fig. 5; Table 5). The connectivity of these ancillary structures to key parts of the prefrontal cortex is important for executive function and may thus influence performance on the WCST. These findings suggest that decreased executive function may be, at least in part, a consequence of disequilibrium in the local and global/interhemispheric processing arising from disorganization of GM cytoarchitecture. The extensive differences in lateralization noted here are likely to relate to abnormal organization of functionally known brain networks.

Limitations and Future Directions

Several limitations of the present study must be considered. First, the study examines a limited sample size and has a purely cross-sectional study design. Whereas the increase in sample homogeneity is likely to increase the statistical power of this study, further work will be needed to establish whether current findings extend to patients of different age, ethnicity, or gender. The observed decreased lateralization may be a progressive pathology of SZ and therefore be specific to age or disease duration. Previous literature has demonstrated that sex, age, and handedness differences can have a confounding effect not only on SZ neuropathology but also on lateralization (Goldstein et al. 2002; Vernooij et al. 2007; Deep-Soboslay et al. 2010; Tomasi and Volkow 2012; Cropley et al. 2017). Thus, future studies are needed to examine microstructural lateralization in larger and more diverse SZ populations. Second, we did not control for antipsychotic medications which could affect microstructural abnormalities. We note that lateralization deficits using volumetric or functional measurements have also been observed in first-episode patients (Bleich-Cohen et al. 2009; Sheng et al. 2013), suggesting that they may occur independently of medication. Medication nonadherence, rather than the medication use, has recently been proposed as a cause of decreased intracortical myelin (Tishler et al. 2018). Third, the voxel size used in this study is relatively large, and thus data presented here is likely to be to some degree affected by partial volume averaging. However, we show that MK metrics do not significantly correlate with measures of cortical thickness in either SZ or HC groups, suggesting that partial volume averaging likely does not affect our results (Supplementary Table 2). Future

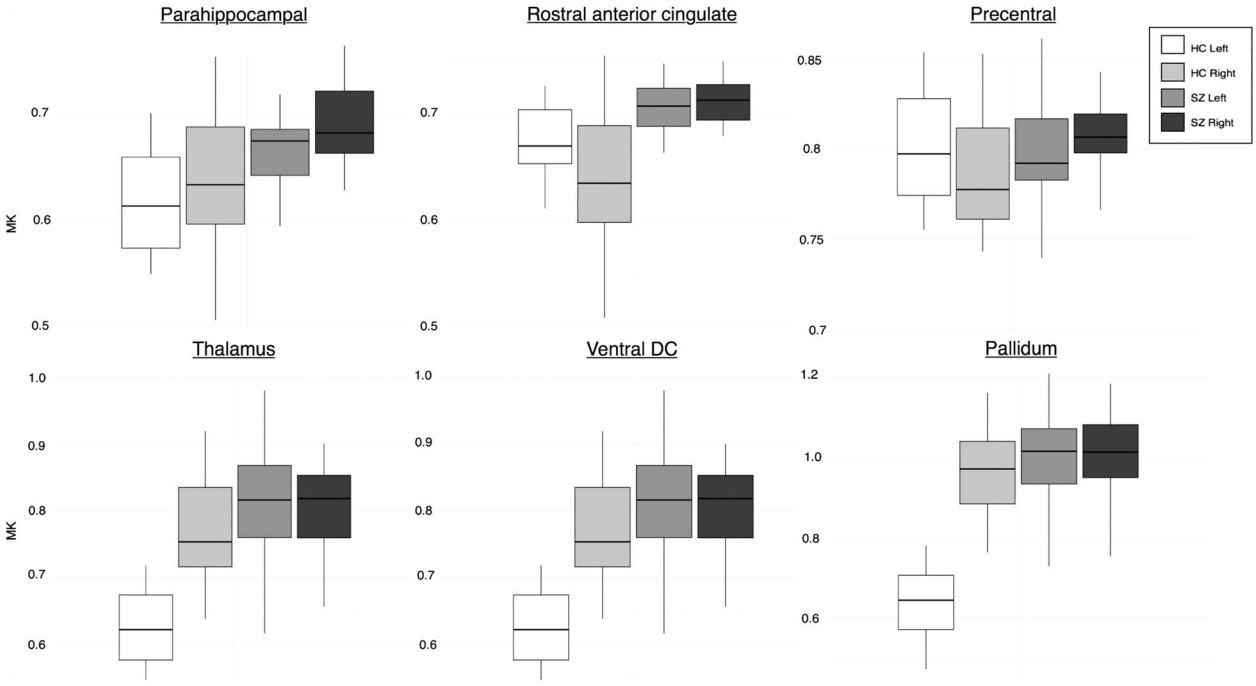

Figure 6. MK values of a sub-set of cortical and subcortical ROIs with significantly different μLI ($P < 0.001$) demonstrating the patterns of lateralization between hemispheres in HC and SZ groups. Color indicates group and hemisphere (HC left—white, HC right—light gray, SZ left—medium gray, SZ right—dark gray). A greater increase in MK is observed in the non-dominant hemisphere in SZ. The top row of cortical ROIs shows that the differences in lateralization in SZ are due to a range of asymmetry patterns including reduced asymmetry but in the same direction as HC (parahippocampal), total loss of asymmetry (rostral anterior cingulate), and reversed asymmetry in comparison with HC (precentral).

studies will be necessary to further confirm our findings and to assess the effects of different diffusion acquisition parameters as well as the effects of the parcellation scheme on the cortical microstructural asymmetry metrics' differences in SZ. Last, we suggest that a multimodal, integrative approach that examines asymmetry changes across both GM and white matter may prove informative in better discriminating the microstructural substrates that are affected in SZ and how these substrates differ between hemispheres. For example, myelin mapping (Alexander et al. 2012; Tishler et al. 2018) may be used to quantify cortical myelination bilateral alterations in SZ. Several white matter–specific advanced diffusion methods that are assumed to better discriminate between features such as axonal density, myelination, and inflammation such as NODDI and diffusion-based spectrum imaging have been recently proposed (Ferizi et al. 2015; Lazar 2017) and may provide more detailed information on the precise changes occurring in SZ GM. The strong relationship between white matter and GM architecture (Zikopoulos et al. 2018) suggests that white matter metrics may also indirectly give information about corresponding GM microstructural properties such as neuronal density.

Conclusion

GM microstructural lateralization is substantially reduced in SZ and may reflect a less efficient brain organization that results in impaired cognitive function. Differences in lateralization appear to arise from tissue changes at a microstructural level although future work will be needed to define the specific tissue alterations involved. Inclusion of GM markers of microstructure such as MK into computational models of brain function may be instrumental in better defining neural dysfunction mechanisms of SZ and may ultimately contribute to improved diagnosis and treatment.

Supplementary Material

Supplementary material is available at *Cerebral Cortex* online.

Funding

National Institute of Mental Health awards (grants R21 MH085228 and R01 MH108962).

Notes

We greatly thank all of our participants for their help with this study and ResearchMatch and Bellevue Inspires Institute for supporting our recruitment efforts. *Conflict of Interest*: None declared.

References

Alary M, Delcroix N, Leroux E, Razafimandimby A, Brazo P, Delamillieure P, Dollfus S. 2013. Functional hemispheric lateralization for language in patients with schizophrenia. *Schizophr Res*. 149:42–47.

Alexander AL, Hurley SA, Samsonov AA, Adluru N, Hosseinbor AP, Mossahebi P, Tromp DPM, Zakszewski E, Field AS. 2012. Characterization of cerebral white matter properties using

quantitative magnetic resonance imaging stains. *Brain Connect*. 1:430–436.

Anderson B, Southern BD, Powers RE. 1999. Anatomic asymmetries of the posterior superior temporal lobes: a postmortem study. *Neuropsychiatry Neuropsychol Behav Neurol*.

Artiges E, Martinot JL, Verdys M, Attar-Levy D, Mazoyer B, Tzourio N, Giraud MJ, Paillere-Martinot ML. 2000. Altered hemispheric functional dominance during word generation in negative schizophrenia. *Schizophr Bull*. 26:709–721.

Bester M, Jensen JH, Babb JS, Tabesh A, Miles L, Herbert J, Grossman RI, Inglese M. 2015. Non-Gaussian diffusion MRI of gray matter is associated with cognitive impairment in multiple sclerosis. *Mult Scler*. 21:935–944.

Bleich-Cohen M, Hendler T, Kotler M, Strous RD. 2009. Reduced language lateralization in first-episode schizophrenia: an fMRI index of functional asymmetry. *Psychiatry Res*. 171: 87–92.

Byne W, Buchsbaum MS, Mattiace LA, Hazlett EA, Kemether E, Elhakem SL, Purohit DP, Haroutunian V, Jones L. 2002. Postmortem assessment of thalamic nuclear volumes in subjects with schizophrenia. *Am J Psychiatry*. 159:59–65.

Casanova MF, Kreczmanski P, Trippe J, Switala A, Heinsen H, Steinbusch HWM, Schmitz C. 2008. Neuronal distribution in the neocortex of schizophrenic patients. *Psychiatry Res*. 158:272–275.

Chance SA. 2014. The cortical microstructural basis of lateralized cognition: a review. *Front Psychol*. 5:1–8.

Chance SA, Casanova MF, Switala AE, Crow TJ. 2008. Auditory cortex asymmetry, altered minicolumn spacing and absence of ageing effects in schizophrenia. *Brain*. 131:3178–3192.

Cropley VL, Klauser P, Lenroot RK, Bruggemann J, Sundram S, Bousman C, Pereira A, Di Biase MA, Weickert TW, Weickert CS *et al*. 2017. Accelerated gray and white matter deterioration with age in schizophrenia. *Am J Psychiatry*. 174:286–295.

Crow TJ, Ball J, Bloom S, Brown R, Bruton CJ, Colter N, Frith CD, Johnstone EC, Owens DG, Roberts GW. 1989. Schizophrenia as an anomaly of development of cerebral asymmetry: a postmortem study and a proposal concerning the genetic basis of the disease. *Arch Gen Psychiatry*. 46:1145–1150.

Cullen TJ, Walker MA, Eastwood SL, Esiri MM, Harrison PJ, Crow TJ. 2006. Anomalies of asymmetry of pyramidal cell density and structure in dorsolateral prefrontal cortex in schizophrenia. *Br J Psychiatry*. 188:26–31.

Das SK, Wang JL, Bing L, Bhetuwal A, Yang HF. 2017. Regional values of diffusional kurtosis estimates in the healthy brain during normal aging. *Clin Neuroradiol*. 27:283–298.

Deep-Soboslay A, Hyde TM, Callicott JP, Lener MS, Verchinski BA, Apud JA, Weinberger DR, Elvevåg B. 2010. Handedness, heritability, neurocognition and brain asymmetry in schizophrenia. *Brain*. 133:3113–3122.

Desikan RS, Segonne F, Fischl B, Quinn BT, Dickerson BC, Blacker D, Buckner RL, Dale AM, Maguire RP, Hyman BT *et al*. 2006. An automated labeling system for subdividing the human cerebral cortex on MRI scans into gyral based regions of interest. *Neuroimage*. 31:968–980.

Di Rosa E, Crow TJ, Walker MA, Black G, Chance SA. 2009. Reduced neuron density, enlarged minicolumn spacing and altered ageing effects in fusiform cortex in schizophrenia. *Psychiatry Res*. 166:102–115.

Ferizi U, Schneider T, Witzel T, Wald LL, Zhang H, Wheeler-Kingshott CAM, Alexander DC. 2015. White matter compartment models for in vivo diffusion MRI at 300mT/m. *Neuroimage*.

Fischl B, Dale AM. 2000. Measuring the thickness of the human cerebral cortex from magnetic resonance images. *Proc Natl Acad Sci*. 97:11050–11055.

Geschwind N, Levitsky W. 1968. Human brain: left-right asymmetries in temporal speech region. *Science*. 161:186–187.

Goldstein JM, Seidman LJ, O'Brien LM, Horton NJ, Kennedy DN, Makris N, Caviness VS, Faraone SV, Tsuang MT. 2002. Impact of normal sexual dimorphisms on sex differences in structural brain abnormalities in schizophrenia assessed by magnetic resonance imaging. *Arch Gen Psychiatry*. 59:154–164.

Guglielmetti C, Veraart J, Roelant E, Mai Z, Daans J, Van Audekerke J, Naeyaert M, Vanhoutte G, Palacios R D Y, Praet J *et al*. 2016. Diffusion kurtosis imaging probes cortical alterations and white matter pathology following cuprizone induced demyelination and spontaneous remyelination. *Neuroimage*. 125:7–14.

Halpern ME. 2005. Lateralization of the vertebrate brain: taking the side of model systems. *J Neurosci*. 25:10351–10357.

Harrison PJ. 2000. Postmortem studies in schizophrenia. *Dialogues Clin Neurosci*. 2:349–357.

Hecht D. 2010. Depression and the hyperactive right-hemisphere. *Neurosci Res*. 68:77–87.

Helpern JA, Adisetiyo V, Falangola MF, Hu C, Di Martino A, Williams K, Castellanos FX, Jensen JH. 2011. Preliminary evidence of altered gray and white matter microstructural development in the frontal lobe of adolescents with attention-deficit hyperactivity disorder: a diffusional kurtosis imaging study. *J Magn Reson Imaging*. 33:17–23.

Hollingshead AB. 2011. Four factor index of social status. *Yale J Sociol*. 8:21–51.

Hutsler J, Galuske RA. 2003. Hemispheric asymmetries in cerebral cortical networks. *Trends Neurosci*. 26:429–433.

Ilonen T, Taiminen T, Lauerma H, Karlsson H, Helenius HYM, Tuimala P, Leinonen KM, Wallenius E, Salokangas RKR. 2000. Impaired Wisconsin card sorting test performance in first-episode schizophrenia: resource or motivation deficit? *Compr Psychiatry*. 41:385–391.

Jenkinson M, Beckmann CF, Behrens TE, Woolrich MW, Smith SM. 2012. FSL. *Neuroimage*. 62:782–790.

Jensen JH, Helpern JA, Ramani A, Lu H, Kaczynski K. 2005. Diffusional kurtosis imaging: the quantification of non-Gaussian water diffusion by means of magnetic resonance imaging. *Magn Reson Med*. 53:1432–1440.

Jovicich J, Marizzoni M, Sala-Llonch R, Bosch B, Bartrés-Faz D, Arnold J, Benninghoff J, Wiltfang J, Roccatagliata L, Nobili F *et al*. 2013. Brain morphometry reproducibility in multicenter 3T MRI studies: a comparison of cross-sectional and longitudinal segmentations. *Neuroimage*.

Kawasaki Y, Maeda Y, Suzuki M, Urata K, Higashima M, Kiba K, Yamaguchi N, Matsuda H, Hisada K. 1993. SPECT analysis of regional cerebral blood flow changes in patients with schizophrenia during the Wisconsin card sorting test. *Schizophr Res*. 10:109–116.

Lazar M, Boada F, Malaspina D, Gonen O. 2015. Altered cortical microstructure in shizophrenia: a diffusional kurtosis imaging study. In Proceedings of the 23rd Annual Meeting of International Society for Magnetic Resonance in Medicine, Toronto, Ontario, Canada: International Society for Magnetic Resonance in Medicine p. 3551.

Lazar M, Boudzinskaia M, Meye E, Malaspina D, James B, Gonen O. 2017. Altered hippocampus microstructure in shizophrenia: a diffusion kurtosis imaging and magnetic resonance spectroscopy imaging study. In the Proceedings of the 24th

Annual Meeting of International Society for Magnetic Resonance in Medicine, Singapore: International Society for Magnetic Resonance in Medicine p. 4229.

Lazar M. 2017. Working memory: how important is white matter? *Neuroscientist*.

Lee CY, Tabesh A, Nesland T, Jensen JH, Helpern JA, Spampinato MV, Bonilha L. 2014. Human brain asymmetry in microstructural connectivity demonstrated by diffusional kurtosis imaging. *Brain Res*. 1588:73–80.

Lee SH, Kubicki M, Asami T, Seidman LJ, Goldstein JM, Mesholam-Gately RI, McCarley RW, Shenton ME. 2013. Extensive white matter abnormalities in patients with first-episode schizophrenia: a diffusion tensor imaging (DTI) study. *Schizophr Res*. 143:231–238.

Leemans A, Jones DK. 2009. The B-matrix must be rotated when correcting for subject motion in DTI data. *Magn Reson Med*. 61:1336–1349.

Liu H, Zhang L, Xi Q, Zhao X, Wang F, Wang X, Men W, Lin Q. 2018. Changes in brain lateralization in patients with mild cognitive impairment and Alzheimer's disease: a resting-state functional magnetic resonance study from Alzheimer's disease neuroimaging initiative. *Front Neurol*. 9:1–8.

McKenna F, Miles L, Lazar M. 2018. Increased Diffusion Kurtosis of Gray Matter in Schizophrenia. In the Proceedings of the Advanced Imaging Innovation and Research i2i Workshop. New York (NY): i2iWorkshop p. 1.

Molina V, Lubeiro A, Soto O, Rodriguez M, Álvarez A, Hernández R, de Luis-García R. 2017. Alterations in prefrontal connectivity in schizophrenia assessed using diffusion magnetic resonance imaging. *Prog Neuropsychopharmacol Biol Psychiatry*. 76:107–115.

Oertel-Knochel V, Linden DE. 2011. Cerebral asymmetry in schizophrenia. *Neuroscientist*. 17:456–467.

Oertel V, Knochel C, Rotarska-Jagiela A, Schonmeyer R, Lindner M, van de Ven V, Haenschel C, Uhlhaas P, Maurer K, Linden DEJ. 2010. Reduced laterality as a trait marker of schizophrenia–evidence from structural and functional neuroimaging. *J Neurosci*. 30:2289–2299.

Okada N, Fukunaga M, Yamashita F, Koshiyama D, Yamamori H, Ohi K, Yasuda Y, Fujimoto M, Watanabe Y, Yahata N *et al*. 2016. Abnormal asymmetries in subcortical brain volume in schizophrenia. *Mol Psychiatry*. 21:1460–1466.

Park HJ, Westin CF, Kubicki M, Maier SE, Niznikiewicz M, Baer A, Frumin M, Kikinis R, Jolesz FA, McCarley RW *et al*. 2004. White matter hemisphere asymmetries in healthy subjects and in schizophrenia: a diffusion tensor MRI study. *Neuroimage*. 23:213–223.

Quan M, Lee SH, Kubicki M, Kikinis Z, Rathi Y, Seidman LJ, Mesholam-Gately RI, Goldstein JM, McCarley RW, Shenton ME *et al*. 2013. White matter tract abnormalities between rostral middle frontal gyrus, inferior frontal gyrus and striatum in first-episode schizophrenia. *Schizophr Res*. 145:1–10.

Raffard S, Bayard S. 2012. Understanding the executive functioning heterogeneity in schizophrenia. *Brain Cogn*. 79:60–69.

Ragland JD, Yoon J, Minzenberg MJ, Carter CS. 2007. Neuroimaging of cognitive disability in schizophrenia: search for a pathophysiological mechanism. *Int Rev Psychiatry*. 19:419–429.

Renteria ME. 2012. Cerebral asymmetry: a quantitative, multifactorial, and plastic brain phenotype. *Twin Res Hum Genet*. 15:401–413.

Ribolsi M, Daskalakis ZJ, Siracusano A, Koch G. 2014. Abnormal asymmetry of brain connectivity in schizophrenia. *Front Hum Neurosci*. 8:1–11.

Riehemann S, Volz HP, Stützer P, Smesny S, Gaser C, Sauer H. 2001. Hypofrontality in neuroleptic-naive schizophrenic patients during the Wisconsin card sorting test–a fMRI study. *Eur Arch Psychiatry Clin Neurosci*. 251:66–71.

Royer C, Delcroix N, Leroux E, Alary M, Razafimandimby A, Brazo P, Delamillieure P, Dollfus S. 2015. Functional and structural brain asymmetries in patients with schizophrenia and bipolar disorders. *Schizophr Res*. 161:210–214.

Rüsch N, Spoletini I, Wilke M, Bria P, Di Paola M, Di Iulio F, Martinotti G, Caltagirone C, Spalletta G. 2007. Prefrontal-thalamic-cerebellar gray matter networks and executive functioning in schizophrenia. *Schizophr Res*. 93:79–89.

Russell JM, Early TS, Patterson JC, Martin JL, Villanueva-Meyer J, McGee MD. 1997. Temporal lobe perfusion asymmetries in schizophrenia. *J Nucl Med*. 38:607–612.

Sasabayashi D, Takayanagi Y, Nishiyama S, Takahashi T, Furuichi A, Kido M, Nishikawa Y, Nakamura M, Noguchi K, Suzuki M. 2017. Increased frontal gyrification negatively correlates with executive function in patients with first-episode schizophrenia. *Cereb Cortex*. 27:2686–2694.

Scheel M, Prokscha T, Bayerl M, Gallinat J, Montag C. 2013. Myelination deficits in schizophrenia: evidence from diffusion tensor imaging. *Brain Struct Funct*. 218:151–156.

Schmitz J, Fraenz C, Schlüter C, Friedrich P, Jung RE, Güntürkün O, Genç E, Ocklenburg S. 2019. Hemispheric asymmetries in cortical gray matter microstructure identified by neurite orientation dispersion and density imaging. *Neuroimage*. 189:667–675.

Selemon LD, Goldman-Rakic PS. 1999. The reduced neuropil hypothesis: a circuit based model of schizophrenia. *Biol Psychiatry*.

Selemon LD, Rajkowska G, Goldman-Rakic PS. 1995. Abnormally high neuronal density in the schizophrenic cortex: a morphometric analysis of prefrontal area 9 and occipital area 17. *Arch Gen Psychiatry*. 52:805–818.

Sheng J, Zhu Y, Lu Z, Liu N, Huang N, Zhang Z, Tan L, Li C, Yu X. 2013. Altered volume and lateralization of language-related regions in first-episode schizophrenia. *Schizophr Res*. 148:168–174.

Spitzer R, Williams J, Gibbon M, First M. 1994. *Structured clinical interview for DSM-IV*. Encyclopedia of Behavioral Medicine, Springer-Verlag New York (NY). pp. 1919–1920.

Steiner J, Mawrin C, Ziegeler A, Bielau H, Ullrich O, Bernstein HG, Bogerts B. 2006. Distribution of HLA-DR-positive microglia in schizophrenia reflects impaired cerebral lateralization. *Acta Neuropathol*. 112:305–316.

Steven AJ, Zhuo J, Melhem ER. 2014. Diffusion kurtosis imaging: an emerging technique for evaluating the microstructural environment of the brain. *Am J Roentgenol*. 202.

Tabesh A, Jensen JH, Ardekani BA, Helpern JA. 2011. Estimation of tensors and tensor-derived measures in diffusional kurtosis imaging. *Magn Reson Med*. 65:823–836.

Takao H, Abe O, Yamasue H, Aoki S, Kasai K, Ohtomo K. 2010. Cerebral asymmetry in patients with schizophrenia: a voxel-based morphometry (VBM) and diffusion tensor imaging (DTI) study. *J Magn Reson Imaging*. 31:221–226.

Tishler TA, Bartzokis G, Lu PH, Raven EP, Khanoyan M, Kirkpatrick CJ, Pyle MH, Villablanca JP, Altshuler LL, Mintz J *et al*. 2018. Abnormal trajectory of intracortical myelination in schizophrenia implicates white matter in disease pathophysiology and the therapeutic mechanism of action of antipsychotics. *Biol Psychiatry Cogn Neurosci Neuroimaging*. 3:454–462.

Tomasi D, Volkow ND. 2012. Laterality patterns of brain functional connectivity: gender effects. *Cereb Cortex*. 22:1455–1462.

Uranova NA, Vikhreva OV, Rachmanova VI, Orlovskaya DD. 2011. Ultrastructural alterations of myelinated fibers and oligodendrocytes in the prefrontal cortex in schizophrenia: a postmortem morphometric study. *Schizophr Res Treatment*. 2011:1–13.

Vernooij MW, Smits M, Wielopolski PA, Houston GC, Krestin GP, van der Lugt A. 2007. Fiber density asymmetry of the arcuate fasciculus in relation to functional hemispheric language lateralization in both right- and left-handed healthy subjects: a combined fMRI and DTI study. *Neuroimage*. 35:1064–1076.

Wang J, Lin W, Lu C, Ng S. 2011. Parkinson disease: diagnostic utility of diffusion kurtosis imaging. *Radiology*. 261 :210–216.

Wonderlick JS, Ziegler DA, Hosseini-Varnamkhasti P, Locascio JJ, Bakkour A, van der Kouwe A, Triantafyllou C, Corkin S, Dickerson BC. 2009. Reliability of MRI-derived cortical and subcortical morphometric measures: effects of pulse sequence, voxel geometry, and parallel imaging. *Neuroimage*. 44:1324–1333.

Zhang Y, Dai Z, Chen Y, Sim K, Sun Y, Yu R. 2018. Altered intra- and inter-hemispheric functional dysconnectivity in schizophrenia. *Brain Imaging Behav*. 13:1220–1235.

Zhu J, Zhuo C, Qin W, Wang D, Ma X, Zhou Y, Yu C. 2015. Performances of diffusion kurtosis imaging and diffusion tensor imaging in detecting white matter abnormality in schizophrenia. *Neuroimage Clin*. 7:170–176.

Zhuo J, Xu S, Proctor JL, Mullins RJ, Simon JZ, Fiskum G, Gullapalli RP. 2012. Diffusion kurtosis as an in vivo imaging marker for reactive astrogliosis in traumatic brain injury. *Neuroimage*. 59:467–477.

Zikopoulos B, García-Cabezas MÁ, Barbas H. 2018. Parallel trends in cortical gray and white matter architecture and connections in primates allow fine study of pathways in humans and reveal network disruptions in autism. *PLoS Biol*. 16: 1–33.